Effect of Surface Structures on Photocatalytic CO_2 Reduction Using Quantized CdS Nanocrystallites[1]

Hiroaki Fujiwara, Hiroji Hosokawa, Kei Murakoshi, Yuji Wada, and Shozo Yanagida*

Material and Life Science, Graduate School of Engineering, Osaka University, Suita, Osaka 565, Japan

Tadashi Okada

Department of Chemistry, Faculty of Engineering Science, Osaka University, Toyonaka, Osaka 560, Japan

Hisayoshi Kobayashi

Department of Chemical Technology, College of Science and Industrial Technology, Kurashiki University of Science and the Arts, Tsurajima, Kurashiki 712, Japan

Received: May 15, 1997; In Final Form: July 14, 1997[⊗]

A mechanistic investigation on the photocatalytic reduction of CO_2 with hexagonal CdS nanocrystallites prepared in *N*,*N*-dimethylformamide (DMF) was carried out from the standpoint of surface structures of the nanocrystallites. A remarkable increase of photocatalytic activity could be achieved by addition of excess Cd^{2+} to the system. Analysis of the emission behavior depending on the amount of excess Cd^{2+} in the system suggests that the Cd^{2+} addition results in the formation of sulfur vacancies on the surface of nanocrystallites due to the adsorption of excess Cd^{2+} to the surface. The formation of the sulfur vacancies on the surface was supported by in situ Cd K-edge EXAFS analysis of the nanocrystallites in solution as changes in the coordination numbers of cadmium−sulfur and cadmium−oxygen. Theoretical MO calculations using a density functional (DF) method supported the preferential bidentate-type absorption of CO_2 with the Cd atom in the vicinity of the sulfur vacancy.

Introduction

Photocatalytic reductions of CO_2 have attracted much interest to cope with the problems of global warming and depletion of fossil fuels.[2] Recently, effective photocatalysis of quantized semiconductor nanocrystallites such as CdS,[1,3] ZnS,[4] $Cd_xZn_{1+x}S$,[5] and TiO_2[6] have been reported for CO_2 photoreduction. Semiconductor nanocrystallites are characterized by their large surface-to-volume ratios, and their reducing power is originated from the size quantization effect in their electronic structure.[7] In our studies of semiconductor photocatalysis, we suggested the importance of the surface structures of the nanocrystallites in CO_2 photoreductions.[1,3] For example, surface modification by the addition of Zn^{2+} to the system of ZnS nanocrystallites induced remarkable product-switching from formate to CO without losing the efficiency.[3] Similarly, the change of the photocatalytic activity due to the addition of excess Cd^{2+} was also observed in the system of CdS nanocrystallites as an increment of the activity to form CO.[1]

In CO_2 reductions by metal complexes and electrodes, adsorptive interaction between CO_2 molecules and metal center strongly depends on their orbital parentage, charge of metal atom, and microscopic structures of neighboring circumstances. In their systems, it has been reported that η^2-side-on, η^1-C-coordination or η^1-O-end-on structures of interacting CO_2 are explained by back-donation effect, electric exchange repulsion, and Coulomb interaction between the electronic orbitals of CO_2 molecules and metal centers.[8] The steric hindrance due to ligands is also an important factor in determining the interaction between metal center and CO_2 molecules.[9] In the system of metal electrodes for electrochemical reduction of CO_2, electrocatalytic activities were correlated with electronic structures of metals as well as the lattice constant of metal atoms at electrode surface.[10] These results imply that the adsorptive interaction of CO_2 molecules with the surface of semiconductor nanocrystallites also plays a crucial role in determining their photocatalytic activity and must be extremely sensitive to microscopic atom arrangement at the surface. Thus, in situ structural analysis is indispensable in understanding the role of surface structures of nanocrystallites for the effective photoreduction of CO_2 molecules. Recently, we demonstrated that in situ information regarding the microscopic surface structure of CdS and ZnS nanocrystallites becomes available by means of in situ EXAFS measurements for colloidal semiconductor nanocrystallites in DMF.[11,12]

We previously reported that CdS nanocrystallites (CdS−DMF, ca. 4 nm in diameter, hexagonal) prepared in DMF catalyzed effective photoreduction of CO_2 to CO under visible light irradiation ($\lambda > 400$ nm). In this reaction, the efficiency was found to be improved drastically by introducing excess Cd^{2+} into the system.[1] In this paper, we deal with a mechanistic investigation in the photoreduction of CO_2 using CdS nanocrystallites as photocatalysts in view of the changes in surface structures of CdS nanocrystallites induced by addition of excess Cd^{2+} and the interaction of adsorbed CO_2 molecules with the surface. Emission properties and in situ EXAFS analysis provided information on the changes of the surface structures of CdS nanocrystallites in the presence of excess Cd^{2+}. These characteristics were correlated to the photocatalytic activity of the system. In addition, structures of the adsorbed CO_2 molecule on CdS models were evaluated using theoretical molecular orbital (MO) calculations based on the DF method. Finally, reaction mechanisms on the surface were discussed in view of selective adsorption of CO_2 molecules on Cd atoms in vicinity of the sulfur vacancies.

[⊗] Abstract published in *Advance ACS Abstracts,* September 15, 1997.

S1089-5647(97)01621-0 CCC: $14.00

Experimental Section

Preparation of Colloidal CdS Photocatalysts. Colloidal CdS nanocrystallites in DMF (CdS−DMF) were prepared as previously described.[1] H_2S gas was introduced into 10 mL of deaerated DMF (spectral grade, Dojin Chemical Laboratories) solution containing 5 mM of $Cd(ClO_4)_2 \cdot 6H_2O$ (reagent grade, Mitsuwa Pure Chemicals) with stirring on an ice bath at 0 °C. The CdS−DMF solution, which showed a transparent yellow color, was purged with nitrogen for 1 h to remove unreacted H_2S before use. The effect of the excess Cd^{2+} was investigated after adding a DMF solution of cadmium perchlorate into the CdS−DMF solution with stirring for 30 min on an ice bath at 0 °C. Excess amount of Cd^{2+} was indicated by a ratio of excess Cd^{2+} concentration to the diatomic concentration (2.5 mM) of CdS nanocrystallites. The systems of CdS−DMF containing excess 0.2 and 0.4 molar ratio of Cd^{2+} were abbreviated as CdS−DMF/Cd0.2 and CdS−DMF/Cd 0.4, respectively.

Experimental Conditions of CdS−DMF-Catalyzed Photoreactions. Photoreductions of CO_2 were carried out as previously described.[1] CO_2 was introduced to a DMF solution (2 mL) containing CdS nanocrystallites (2.5 mM, diatomic) as a photocatalyst and distilled triethylamine (TEA, 1 M) as an electron donor. The solution in a closed Pyrex tube (8 mm diameter) was irradiated with a 300 W halogen tungsten lamp using an optical filter of a saturated aqueous sodium nitrite solution ($\lambda > 400$ nm) under cooling on a water bath (25 °C).

Gas analysis of CO and H_2 was carried out using gas chromatography with an active carbon column. Formic acid analysis was performed using HPLC with an ion-exchange column. The details of these analysis are described elsewhere.[1]

Emission Spectra and Lifetime Measurements. Emission measurements were carried out using a quartz cell with optical path length of 10 mm. A sample solution was introduced into the cell and then degassed by Ar (99.99%). The cell was capped and sealed for emission measurements. Steady-state emission spectra were recorded with a fluorescence spectrophotometer (Model 850, Hitachi Ltd.).

Emission lifetime measurements were carried out as follows. Excitation pulses were produced from a frequency-doubled mode-locked Ti:sapphire laser (Spectra-Physics, Tsunami, $\lambda =$ 730−820 nm, fwhm 60−100 fs, 400−700 mW (8.2 MHz)) pumped by an Ar^+ laser (Spectra-Physics BeamLok 2060, 6−7 W). The samples were excited at $\lambda = 400$ nm by the second harmonics of a mode-locked Ti:sapphire laser generated with BBO crystal at room temperature. The emission decay curve was measured by using a time-correlated single-photon-counting system (Hamamatsu Photonics R3809U) with a time resolution of about 40 ps/channel. The response of the system was integrated for 1 h for each sample. The lifetime of the emission was determined by a third-exponential decay law of the region between 0 and 10 ns.

EXAFS Measurements and Analysis. Cd K-edge (26710 eV) EXAFS measurements were performed on the BL-14A at the Photon Factory of the National Laboratory for High Energy Physics. The details of these analysis are described elsewhere.[11,13] The X-ray energy for solution samples was scanned with an integration time of 8 s and at steps of 1 eV in a XANES region (26 300−26 800 eV) and of 2 eV in a EXAFS region (26 800−27 600 eV). For powder samples, 2 and 3 eV steps with an integration time of 6 s were used in the XANES and EXAFS regions, respectively. The concentration of Cd atoms in DMF solution was 15 mM. For powder samples, pellets of Cd compounds (0.4 mmol cm^{-2}, 2 mm thick) mixed with polyethylene (reagent grade, Wako Pure Chemicals) as a binder were used.

The EXAFS data were analyzed according to previously described standard procedures.[11] The EXAFS spectra were extracted with normalization of the edge step, interpolation onto a photoelectron momentum vector, and subtraction of the postedge background. The resulting EXAFS oscillations were multiplied by k^3 and Fourier filtered with Hamming windows. The Fourier-filtered data were analyzed by nonlinear least-squares curve-fitting techniques. Further details of the procedures have been presented elsewhere. Standard samples of bulk CdS powder (99.999%, Aldrich) and a DMF solution of $Cd(ClO_4)_2 \cdot 6H_2O$ (reagent grade, Mitsuwa Pure Chemicals) provided the reference parameters for the first shell of Cd−S and of Cd−O, respectively.

Theoretical Calculations. The geometrical structure of adsorbed CO_2 on the CdS surface was examined by a theoretical calculation using the DF program "deMon".[14] The orientation and internal structure of the CO_2 molecule on the CdS catalyst surface, which was modeled by $Cd_3S_3H_8$ and $Cd_3S_2H_8$ clusters to represent the sulfur-vacancy-free catalyst and the catalyst with sulfur vacancy, respectively, were optimized. The atomic coordinates of the model cluster were taken from the hexagonal structure of the CdS crystal. The nearest Cd−S distance is 2.53 Å, and the sulfur plane is 0.84 Å higher than the cadmium plane. Hydrogen atoms were used to saturate the valence of the peripheral Cd and S atoms.

The orbital basis sets used for Cd, S, C, O, and H atoms were (63321/53211*/531$^+$), (311/211/1), (5211/411), (5211/411), and (41) or (3), respectively. For sulfur, the 1s to 2p electrons were replaced by a model core potential, and the polarization δ function was included. Both the polarization and diffuse σ and π functions were added to the C and O atoms. Basis sets (41) and (3) were used for the H atoms representing Cd and S. Basis set (41) reflects that the orbital on Cd is more diffuse than that on S. The atoms outside the cluster were approximated by point charges, and 294 points were considered to cover the hemispherical region of radius 10 Å. The magnitude of charges was set at 0.3 (+0.3 for Cd and −0.3 for S) after consulting the results of our CdS slab calculation. The quality of the bases was equal to or greater than the split valence level. The uncontracted auxilliary fitting functions of types, (10/5/5), (5/3/3), (7/2/2), (7/2/2), and (6/1/1) were used for the Cd, S, C, O, and H atoms, respectively. The local potentials proposed by Vosko, Wilk, and Nusair were used throughout the calculations.

Results and Discussion

Effect of Excess Cd^{2+} on CdS-Catalyzed Photoreduction of CO_2. In photoreduction of CO_2 with CdS−DMF, the formation of CO was observed after induction period for 30 min as reported in the previous paper.[1] In addition, we found that the photoreduction activity largely depended on the concentration of excess Cd^{2+} in the system.[1] Figure 1 shows the effect of excess Cd^{2+} on the photoproduction of CO after 1 h photoreaction. The CO formation was increased by a factor of 2 when 0.2 equivalent amount of excess Cd^{2+} to the concentration of CdS−DMF was added into the system. Induction period of the CO formation became shorter by the addition of excess Cd^{2+}. The addition of more than 0.2 equivalent of excess Cd^{2+}, however, led to a decrease of the photocatalytic activity. During the reaction with the system containing more than 0.2 equivalent of excess Cd^{2+}, photodarkening of the CdS−DMF solution was observed after 30 min irradiation. The photocatalytic activity of the system containing 0.8 equivalent of excess Cd^{2+} was less than that of

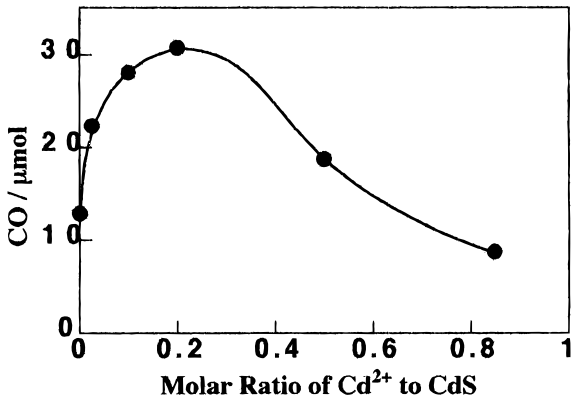

Figure 1. Effect of the addition of excess Cd^{2+} on efficiency of the CdS−DMF-catalyzed CO formation.

the system without addition of excess Cd^{2+}. The formation of HCOOH, CH_3OH, and $(COOH)_2$ was not observed in any systems.

Effect of Excess Cd^{2+} on CdS−DMF Nanocrystallites. *Emission Properties of CdS−DMF.* Figure 2a shows the emission spectra of the CdS−DMF solution by excitation at $\lambda = 400$ nm. The spectra consist of two broad-band peaks at $\lambda = 650$ and 480 nm. Relatively strong emission at λ=650 nm is attributed to radiative recombination at deep trap sites originating from lattice imperfections at the surface, i.e., the surface states, and the emission at $\lambda = 480$ nm is to direct recombination of electron and hole pairs at the bandgap.[15] The relative intensities of the emissions depended on the amount of excess Cd^{2+} in the solution. The emission intensity at $\lambda = 650$ nm increased as excess Cd^{2+} increased up to 0.2 equivalent and then decreased until 1.0 equivalent. This behavior was identical with the results reported by Henglein et al.[16] Relatively large enhancement of the emission at deep trap sites compared with that at the bandgap reflects that lattice imperfections on the surface of nanocrystallites, i.e., surface vacancies,[15a] increase as excess Cd^{2+} is added into the system. It was confirmed that absorption spectrum was not affected by the addition of excess Cd^{2+}, indicating that size growth did not occur in the system under the present conditions. The decrease of the emission at the deep trap sites in the presence of more than 0.2 equivalent of excess Cd^{2+} should be due to the quenching of excited electrons in the reduction of free Cd^{2+} in the solution.[17] This process was supported by the change of the color of the system due to the formation of Cd^0 on the surface of the nanocrystallites under irradiation.

Emission-lifetime measurements in the nanosecond time region were also carried out for the emission at $\lambda = 480$ and 650 nm. Figure 2b shows emission decay curves of CdS−DMF containing various amounts of excess Cd^{2+}. Multiexponential decay behavior was observed for both the emission bands. Decay curves at $\lambda = 480$ nm was much faster than that at $\lambda = 650$ nm. A fast decay component at $\lambda = 480$ nm less than the order of nanoseconds was attributed to the recombination of electrons and holes. A slow decay component at $\lambda = 480$ nm in the order of a few nanoseconds was attributed to thermal detrapping of the electron from the surface states to the conduction band since such thermal activation could enhance the lifetime at the band-edge emission.[7d,15c,18] Figure 3 shows that average lifetimes of the both emission[19] depend on the amount of the added Cd^{2+}. The emission lifetime at $\lambda = 480$ nm increased as excess Cd^{2+} increased up to 0.2 equivalent and then decreased. On the other hand, the lifetime at $\lambda = 650$ nm was not affected in the region below 0.2 equivalent of excess Cd^{2+}. The emission lifetime at $\lambda = 650$ nm gradually decreased

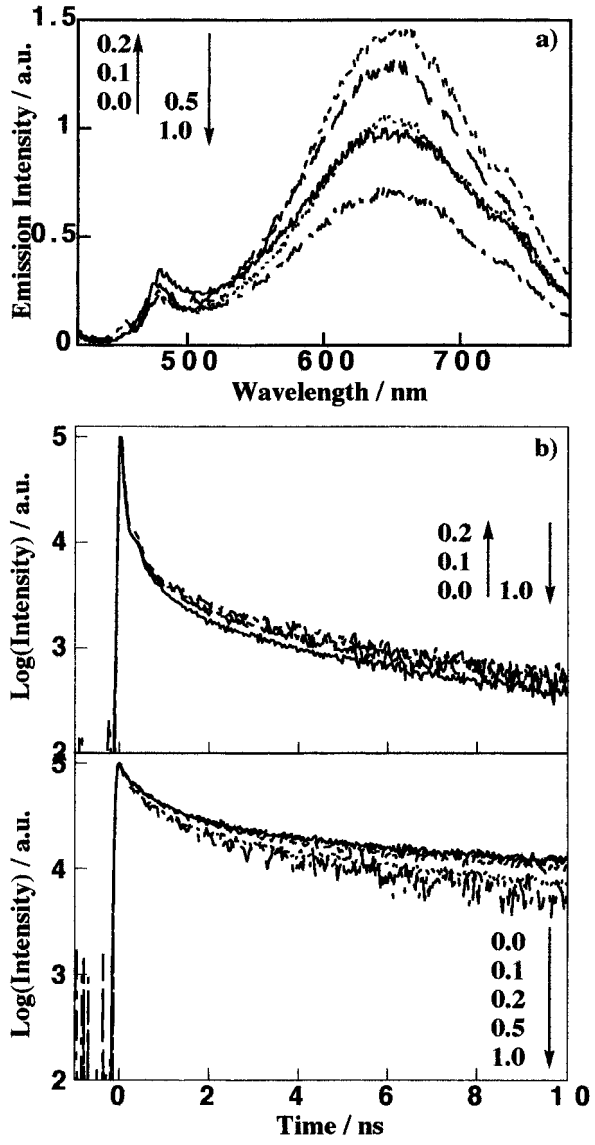

Figure 2. (a) Effect of excess Cd^{2+} addition on emission spectra excited at $\lambda = 400$ nm. (b) Effect of excess Cd^{2+} addition on the emission lifetime excited at $\lambda = 400$ nm (upper spectra were monitored at 480 nm; lower spectra were monitored at 650 nm). Excess amount of Cd^{2+} was induced with 0.0 (—), 0.1 (− − −), 0.2 (- - -), 0.5 (···) and 1.0 (− · −) equivalent of excess Cd^{2+} to CdS−DMF nanocrystallites.

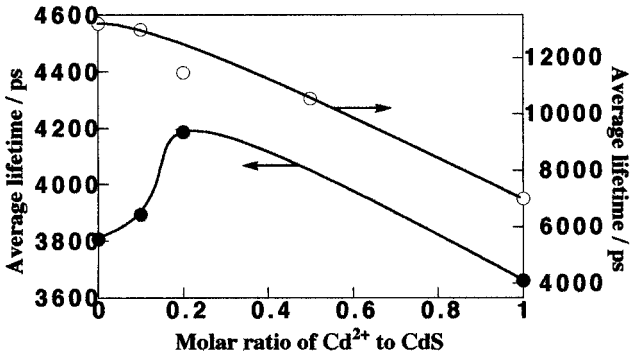

Figure 3. Dependence of excess Cd^{2+} on average lifetime of the emission monitored at $\lambda = 480$ nm (●) and $\lambda = 650$ nm (○).

when more than 0.2 equivalent of excess Cd^{2+} was added. The behavior of the lifetime in the region below 0.2 equivalent of excess Cd^{2+} can be explained by increment of the shallow trap sites. As the shallow trap sites increase, the lifetime at the band-edge emission could be elongated because of the increment of a thermally detrapped electron from the shallow trap sites to

conduction band-edge states. We assumed that the added excess Cd^{2+} form not only the deep trap sites but also the shallow trap sites. Accordingly, the trap sites should be originated from lattice imperfections that should be formed on the surface of CdS−DMF nanocrystallites, as a result of adsorption of excess Cd^{2+}. The effect of the emission intensity and lifetime proved that the maximum number of the trap site was achieved when 0.2 equivalent of excess Cd^{2+} was introduced into the system. Increment of the trap sites affects the emission intensity at $\lambda =$ 650 nm rather than the lifetime of emission. In the system containing more than 0.2 equivalent of excess Cd^{2+}, the decrease of both emission intensity and lifetime suggests that the quenching process leading to a decrease of the trapped electrons could increase in this region. The quenching process might be attributed to the reduction of free Cd^{2+} to Cd^0 in the system.

Surface Structures of CdS−DMF-Based on EXAFS Measurements. EXAFS measurements were carried out to confirm the microscopic surface structure of CdS−DMF in the presence of excess Cd^{2+}. Figure 4a,b shows phase-uncorrected Fourier transforms of k^3-weighted EXAFS for standard samples (bulk CdS powder and a DMF solution of cadmium perchlorate). The peak at 2.09 Å in the Fourier transform (Figure 4a) of EXAFS for bulk CdS powder can be assigned to a four-coordination of sulfur atoms in the CdS crystal lattice. The peak was observed at 1.80 Å in the Fourier transform (Figure 4b) of EXAFS for a DMF solution of cadmium perchlorate. The solvation structure of a DMF solution of cadmium perchlorate has been established to be the six-coordinate octahedral structure.[20] Thus, this main peak at 1.80 Å was assigned to a six-coordination of a DMF oxygen atom to the DMF-solvated Cd^{2+}. Excellent fitting for Fourier-filtered $k^3\chi(k)$ of standard samples (bulk CdS powder and a DMF solution of cadmium perchlorate) was achieved for the Cd−S shell ($R = 5.77\%$) and the Cd−O shell ($R = 8.09\%$) with extraction of the reference parameters[21] and the reported bond lengths of Cd−S (2.542 Å)[22] and Cd−O (2.296 Å)[20] as fixed parameters (Table 1).

Figure 4c shows phase-uncorrected Fourier transform of k^3-weighted EXAFS for a CdS−DMF solution without excess Cd^{2+}. The main peak at 2.05 Å in the transform of CdS−DMF differs from that of bulk CdS (Figure 4b) with respect to the width of the absolute magnitude. These results suggest that the main peak in the transform of EXAFS of CdS−DMF solution is due to scattering not only by sulfur atoms in CdS−DMF nanocrystallites but also by oxygen atoms of DMF molecules solvated to surface Cd atoms of CdS−DMF nanocrystallites as mentioned in the previous paper.[11] As shown in Table 1, analysis of Fourier-filtered $k^3\chi(k)$ of the CdS−DMF solution gave an excellent fitting ($R = 6.43\%$) with a two-shell fit of Cd−O and Cd−S, but not with a one-shell fit of Cd−S. Figure 4d,e shows phase-uncorrected Fourier transforms of k^3-weighted EXAFS for the CdS−DMF/CdX ($X = 0.2$ and 0.4) solutions, respectively. The increment of the intensity in the magnitude as well as the imaginary part was clearly observed. These results suggest that the contribution of the scattering due to the solvating DMF oxygen increased as the amount of excess Cd^{2+} increased. Two-shell fitting for Fourier-filtered $k^3\chi(k)$ of a DMF solution of CdS−DMF/Cd0.2 and CdS−DMF/Cd0.4 gave excellent fitting for CdS−DMF/Cd0.2 ($R = 3.10\%$) and CdS−DMF/Cd0.4 ($R = 9.69\%$) as shown in Table 1.

Figure 5 shows the effect of excess Cd^{2+} on the coordination numbers of Cd−O and Cd−S determined by the EXAFS analysis. As excess Cd^{2+} increased, CN_{Cd-S} decreased and CN_{Cd-O} increased. The changes of CN_{Cd-S} and CN_{Cd-O} of CdS−DMF became more apparent as the added excess Cd^{2+} was increased. It should be noted that the sum of coordination

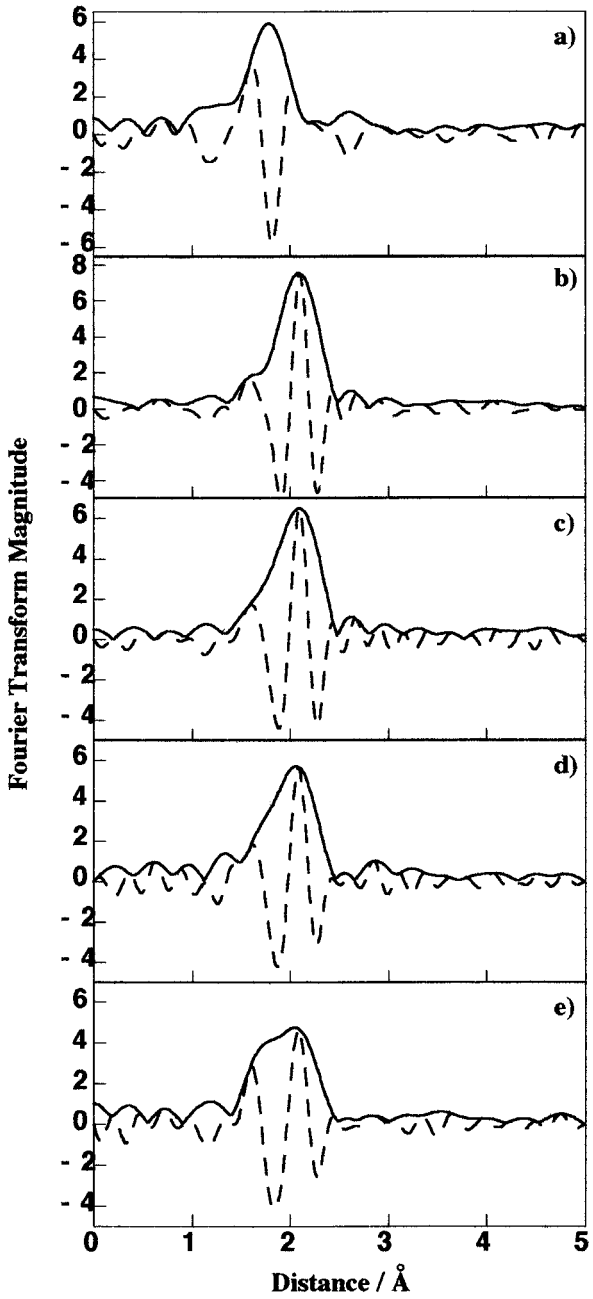

Figure 4. Phase-uncorrected Fourier transforms of $k^3(\chi)$: (a) bulk CdS powder, (b) Cd^{2+} in DMF, (c) CdS−DMF solution, (d) CdS−DMF/Cd0.2, and (e) CdS−DMF/Cd0.4. The k space data ranges used in the transforms were (a) 3.3−13.2 $Å^{-1}$, (b) 3.5−13.2 $Å^{-1}$, (c) 3.55−13.4 $Å^{-1}$, (d) 3.5−13.3 $Å^{-1}$, and (e) 3.45−13.3 $Å^{-1}$. A Hamming window of 5% of the k ranges was used.

numbers, CN_{Cd-S} and CN_{Cd-O}, also depended on the concentration of excess Cd^{2+}. As the amount of excess Cd^{2+} increased, the sum of coordination number increased from 4.0 (CdS−DMF/Cd0.0) to 4.5 (CdS−DMF/Cd0.2) and then 5.2 (CdS−DMF/Cd0.4). The increase in the coordination numbers, CN_{Cd-O}, and the sum of the coordination numbers of CN_{Cd-S} and CN_{Cd-O} indicate that the number of Cd atoms that are solvated by more than one DMF molecule increased as the added excess Cd^{2+} increased.

Such difference in coordination structure due to excess Cd^{2+} was also found in the change of the square of the Debye−Waller factor for Cd−O bonding. It should be noted that the values of the bond length and the square of the Debye−Waller factor for Cd−S bonding were comparable with those of bulk CdS (cf. r, 2.542 Å; σ^2, 0.0061 $Å^2$) and not affected by the amount

TABLE 1: Curve-Fitting Results for Fourier-Filtered $k^3\chi(k)$ Cd K-Edge EXAFS of Cd Compounds[a]

sample	shell	Δr/Å[b]	r/Å[c]	CN[d]	σ^2/Å^2[e]	R/%[f]
$Cd(ClO_4)_2 \cdot 6H_2O$/DMF[g]	Cd−O	1.34−2.20	[2.296][h]	[6][i]	0.0072	8.09
CdS(Ald)[g]	Cd−s	1.43−2.35	[2.542][h]	[4][j]	0.0061	2.77
$CdS(ClO_4)$[k]	Cd−O	1.34−2.48	2.291	0.5	0.0028	6.43
	Cd−S		2.537	3.5	0.0066	
$CdS(ClO_4)$/Cd0.2[k]	Cd−O	1.34−2.48	2.289	1.1	0.0059	3.10
	Cd−S		2.537	3.4	0.0078	
$CdS(ClO_4)$/Cd0.4[k]	Cd−O	1.34−2.48	2.287	2.6	0.0084	9.69
	Cd−S		2.535	2.6	0.0069	

[a] Curve-fitting was performed over of 3.6−12.8 Å^{-1}. [b] The window for the inverse Fourier transform. Hamming window = 0.04 Å^{-1}. [c] Atomic distance. [d] Coordination number. [e] The square of the Debye−Waller factor. [f] Quality of the fit, defined as $\{\sum(k^3\chi_{obsd} - k^3\chi_{calcd})^2/\sum(k^3\chi_{obsd})^2\}^{1/2}$. [g] One-shell fit. [h] Fixed parameter. [i] The reduction factor is 0.907. [j] The reduction factor is 0.863. [k] Two-shell fit. Standard deviations of one-shell fit, $r \pm 0.007$; CN ±1.1; σ^2 ±0.0010 for the Cd−O shell; r ±0.004; CN ±0.6; σ^2 ±0.0015 for the Cd−S shell. Standard deviations of two-shell fit; $r \pm 0.02$; CN ±1.1; σ^2 ±0.0053 for the Cd−O shell; $r \pm 0.005$; CN ±0.7; σ^2 0.0015 for the Cd−S shell.

SCHEME 1

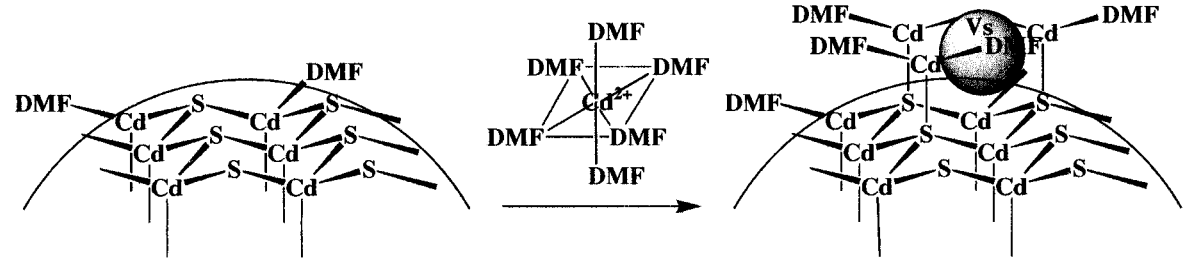

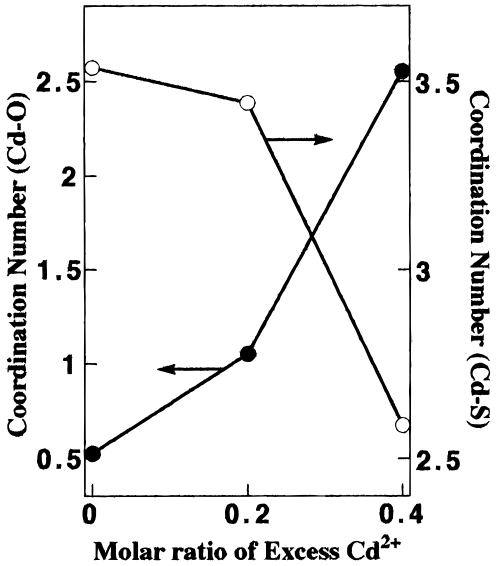

Figure 5. Effect of excess Cd^{2+} addition on the coordination number of Cd−O (●) and Cd−S (○) shell obtained by EXAFS measurement.

of excess Cd^{2+}. The lattice structure of CdS−DMF nanocrystallites in DMF was comparable to that of bulk CdS and is not affected by the surface reaction with excess Cd^{2+}. The square of the Debye−Waller factor of the Cd−O shell in the system of CdS−DMF/Cd0.0 (σ^2, 0.0028 Å^2) is smaller than that in a DMF solution with cadmium perchlorate (σ^2, 0.0072 Å^2) although the bond length of the Cd−O bonding of CdS−DMF was comparable with those of cadmium perchlorate in DMF. The smaller square of the Debye−Waller factor for Cd−O bonding should be originated from the effective solvation of DMF molecule on the surface of CdS nanocrystallites. With an increase of excess Cd^{2+}, the square of the Debye−Waller factor of the Cd−O shell increased and became comparable with that of the Cd−O shell in a DMF solution of cadmium perchlorate. The increment of the values reflects the surface-solvating structure of CdS nanocrystallites which are close to that of Cd^{2+} in DMF. These behavior agrees well with the results of the coordination number of Cd−O shell.

On the basis of these analyses of EXAFS data, we propose that the structure of CdS−DMF nanocrystallites changes as shown in Scheme 1. The Cd−O shell for a DMF solution of cadmium perchlorate have the larger coordination number and Debye−Waller factor than that for a DMF solution of CdS−DMF nanocrystallites. As a result of the adsorption by the DMF-solvated Cd^{2+}, a increase of the coordination number and Debye−Waller factor is considered. When 0.2 equivalent of excess Cd^{2+} was added into the system, the adsorption of Cd^{2+} ions solvated by DMF occurred to the CdS−DMF surface and resulted in the formation of the sulfur surface vacancy on the surface of CdS−DMF nanocrystallites. The change in the coordination number and the square of the Debye−Waller factor of Cd−S and Cd−O shell support such change of the surface structure on CdS−DMF nanocrystallites. Furthermore, the significant change in the Cd−O coordination number of CdS−DMF/Cd 0.4 suggests that the DMF-solvated free Cd^{2+} may exist in the system because the coordination number was larger than the estimated values using the models.[26] The square of the Debye−Waller factor of CdS−DMF/Cd 0.4 also supports the existence of the free Cd^{2+} in the system.

Interaction of CO_2 on Surface of CdS Nanocrystallites. *Emission Properties of CdS−DMF in the Presence of CO_2.* To correlate the photocatalytic activity with the surface structures, interaction between CO_2 molecule and the surface of the CdS−DMF photocatalyst was examined. Figure 6a shows the effect of CO_2 on the emission spectra of a DMF solution of CdS−DMF in the presence of TEA. The emission intensities at λ = 480 and 650 nm increased drastically when CO_2 was introduced into the system. The decay curves of the emission monitored at λ = 480 nm indicated that the emission lifetime was elongated by the addition of CO_2 (Figure 6b). This elongation of the lifetime due to the CO_2 addition was also observed at λ = 650 nm. Although similar results were obtained in the absence of TEA, the effect of CO_2 on the emission was found to be much clearer in the presence of TEA.

These emission reflects the behavior of photogenerated electron and hole pairs on CdS−DMF nanocrystallites. We propose an energy diagram explaining the effect of the addition

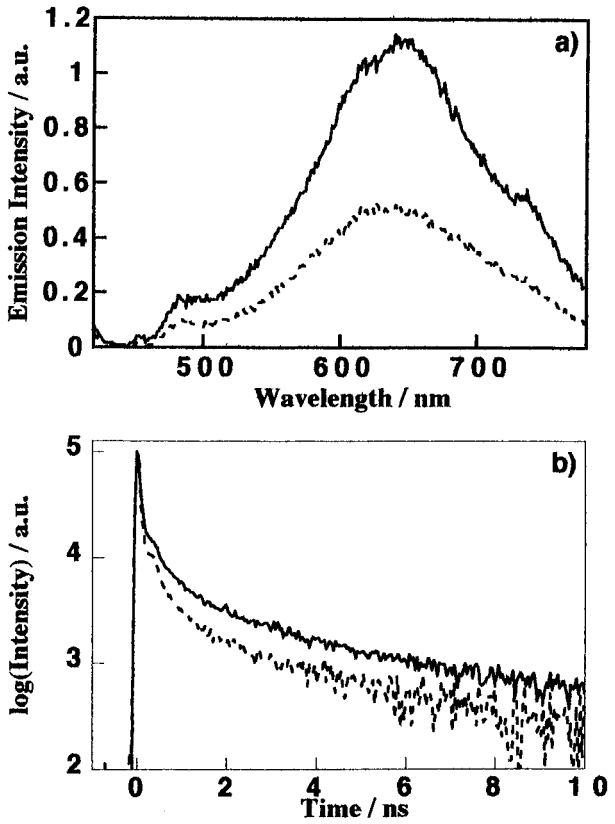

Figure 6. Effect of CO_2 addition on emission properties in the presence of TEA: (a) emission and (b) emission lifetime monitored at $\lambda = 480$ nm.; in the absence (- - -) and the presence (—) of CO_2.

SCHEME 2

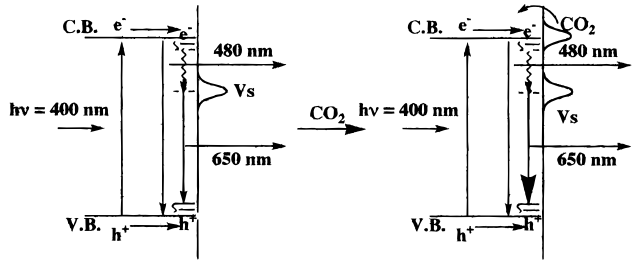

of CO_2 and TEA as schematically shown in Scheme 2. The elongation of the emission in the nanosecond time scale should be attributed to an increase of a thermally detrapped electron on the conduction band of CdS−DMF nanocrystallites, i.e., the adsorbed CO_2 molecule on the surface should create the surface state that can delocalize photoformed electrons. Considering the efficient photoreduction of CO_2 to CO via successive two-electron transfer on CdS−DMF nanocrystallites together with the present emission behavior, we assumed that CO_2 molecules favorably interact with the surface of CdS−DMF nanocrystallites, producing adsorbed $CO_2^{\bullet-}$ on the CdS−DMF surface as an important intermediate, and that the adsorbed $CO_2^{\bullet-}$ reinjects electrons into the conduction band, thus resulting in extending the lifetime of the excited electron. In the previous paper, we reported that the spectrum of $CO_2^{\bullet-}$ trapped with 5,5-dimethyl-1-pyrroline *N*-oxide (DMPO) was observed in the EPR measurement in this system.[23] These adsorbed $CO_2^{\bullet-}$ on the CdS−DMF surface can undergo a successive electron-transfer reaction, resulting in the formation of CO. Thus, the enhancement of the emission intensity and the elongated lifetime of the emission in the presence of CO_2 should be evidence of the strong interaction of CO_2 molecules with the surface of CdS−DMF as observed in the ZnS−DMF systems.[4d]

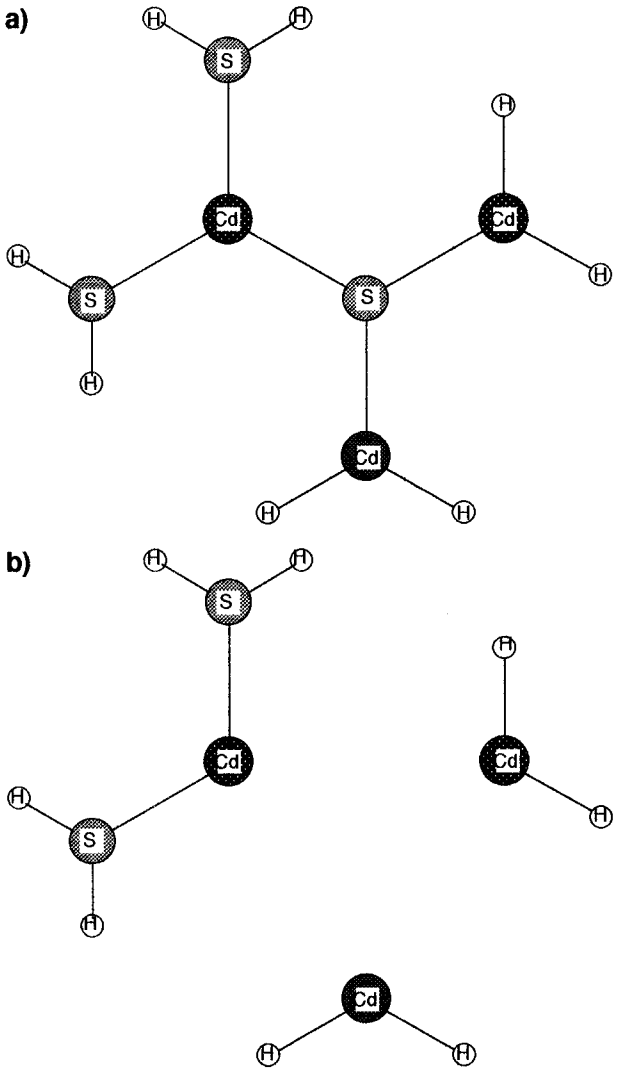

Figure 7. Structure of CdS cluster models (a) $Cd_3S_3H_8$ and (b) $Cd_2S_3H_8$.

Optimized Structures of Adsorbed CO_2 Molecule on CdS. To evaluate the interaction between CO_2 molecules and surfaces of CdS−DMF, theoretical molecular orbital calculations using the DF method were performed. The catalyst surfaces were modeled by $Cd_3S_3H_8$ and $Cd_3S_2H_8$ clusters for a sulfur-vacancy-free surface (ideal surface) and a surface with a sulfur vacancy (S-defect surface), respectively. A surface with a sulfur vacancy model (Figure 7b) was formed by removing the central sulfur atom from the former model (Figure 7a). In calculations, we adapted three models to determine the total energy of the system. The first one is an O-end-on model where CO_2 molecule adsorbs via O atom to the surface as shown in Figure 8a,b. The second one is a C-absorbed model absorbed via C atom as shown in Figure 8c,d. In the third one, CO_2 molecule interacts with the surface via both O and C atom as shown in Figure 8e. We optimized each CO_2-adsorbed structure and derived the total energy of the system with/without S-defect. The third model is available only for the model with S-defect, because the bidentate adsorption via O and C atom was not conceivable on the ideal surface. Furthermore, the states reduced by one-electron, i.e., the electron-accepted model, of the structure and the total energy were also examined. Table 2 summarizes the stabilization energy (ΔE) calculated by the following equation and the atomic charges of the selected atoms estimated by the Mulliken population.

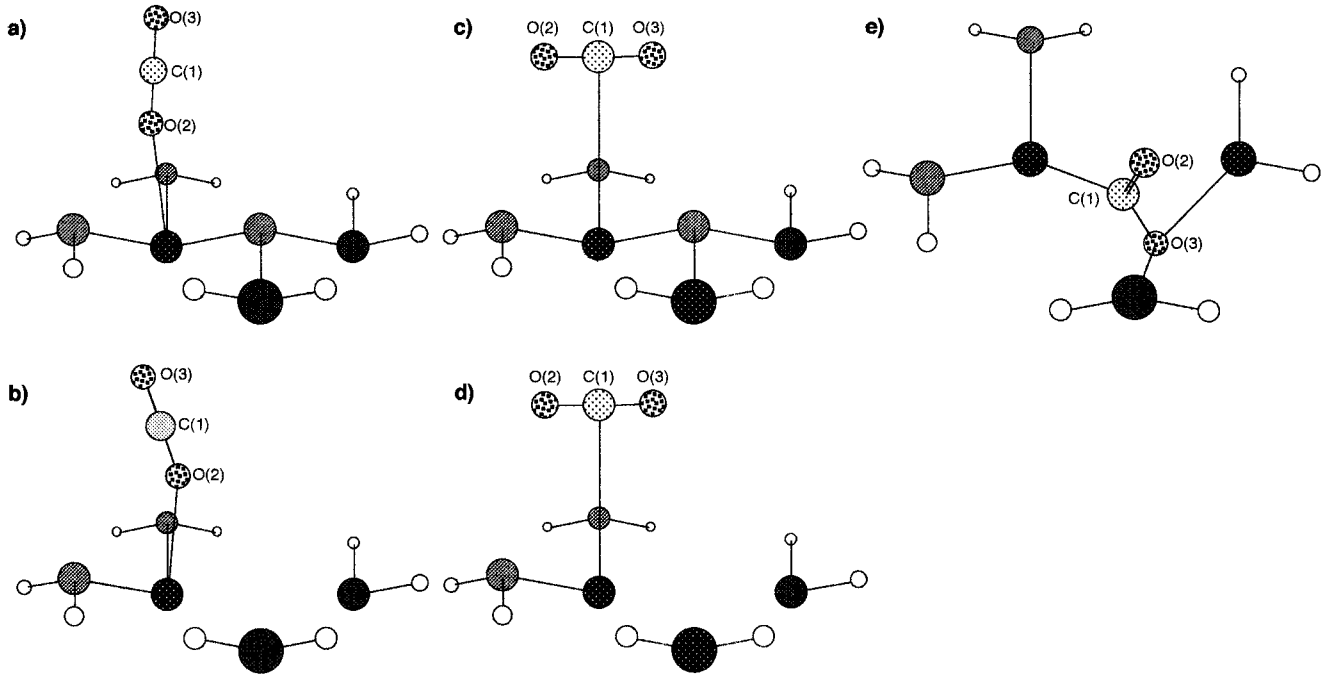

Figure 8. Optimized structures for CO_2 absorption on CdS cluster models: (a) ION, (b) DON, (c) ICN, (d) DCN, and (e) BN.

TABLE 2: Calculation Results (Stabilized Energy, Atomic Distance, Bond Angle, and Charge) for Each Model

model	ION	IOA	DON	DOA	ICN	ICA	DCN	DCA	BN	BA
ΔE (kcal/mol)	−4.066	−3.816	−4.066	−3.878	−1.619	0.449	−0.996	−2.346	−39.782	−50.916
C(1)−O(2)[a]	1.173	1.169	1.179	1.193	1.173	1.169	1.170	1.175	1.247	1.227
C(1)−O(3)[a]	1.167	1.174	1.170	1.190	1.169	1.171	1.170	1.175	1.292	1.342
C(1)−Cd[a,b]	3.947	3.924	3.789	3.650	4.298	4.297	4.300	3.919	2.127	2.155
O(2)−Cd[a,b]	2.829	2.837	2.795	2.757					2.882	2.759
O(3)−Cd[a,b]									3.006	3.112
O−C−O[c]	179.7	178.8	179.5	160.5	179.2	179.0	179.4	171.8	124.0	121.9
Q(CO_2)[d]	+0.075	+0.155	+0.053	−0.180	−0.002	−0.023	+0.001	−0.058	−1.119	−1.314
Q(Cd)[e]	+0.396	−0.114	−0.030	−0.227	−0.402	−0.077	−0.038	−0.268	+0.621	+0.181
Q(S)[f]	−0.480	−0.555			+0.468	−0.550				

[a] Bond distance (angstrom). [b] Cd atom which CO_2 is bonded. [c] Bond angle of CO_2. [d] Total charge distribution of CO_2. [e] Charge distribution of Cd atom which CO_2 is bonded. [f] Charge distribution of S atom which is removed in the defect models.

$$\Delta E = E(\mathrm{CdS/CO_2}) - (E(\mathrm{CdS}) + E(\mathrm{CO_2}))$$

The stabilization energies for the neutral states of O-end-on models (ION, IOA, DON, DOA[24]) and C-adsorbed models (ICN, ICA, DCN, DCA[24]), respectively, were relatively small as shown in Table 2. These results indicate that the interactions between CO_2 and CdS surface are not strong. On the other hand, the stabilization energies for the neutral states of bidentate-type model on the S-defect surface (BN[24]) was calculated to be 39.78 kcal/mol. In the electron-accepting anionic models, the stabilization energy for the O-end-on models and C-adsorbed models was comparable with that of corresponding neutral models. However, the stabilization energy for the electron-accepted model of the bidentate-type adsorption on S-defect surface (BA[24]) increases to 50.92 kcal/mol. These results indicate that the bidentate-type absorption of CO_2 molecule on CdS surface with sulfur vacancies should be more stable than the other types of adsorption.

Generally, the coordination of CO_2 to the transition metals has been reported to have coordination structure such as η^2-side-on, η^1-C-coordination, and η^1-O-end-on of CO_2.[8] In these structures, the adsorption of CO_2 molecule is stabilized by back-donation from metals to CO_2. On the other hand, it was reported that CO_2 is bonded via both C and O ends in the system CO_2/Rh/TiO_2.[25] The carbon atom of CO_2 is bonded to the Rh atom, while the oxygen atom of CO_2 is bonded to the oxygen vacancy of titania surface. In this system, TiO_2 donates an electron to surface Rh atoms, and as a result, the back-donation of electrons from Rh into the π orbital of CO_2, and the formation of partially and negatively charged CO_2 will occur on the surface. Bidentate-type adsorption of CO_2 on the CdS surface with S-vacancy (BN) may be a type of the adsorption corresponding to such adsorption.

The calculations of the bond distances and the charge distribution support the above hypothesis (Table 2). The bond distance of Cd−C and Cd−O in BN and BA models were relatively shorter than those of the other models. The results suggest that CO_2 molecule in BN and BA model should be adsorbed with stronger interaction than CO_2 of the other models. In addition, the calculated C−O bond lengths and the angle of O−C−O of CO_2 molecule in the BN model are almost same as that of $CO_2^{\bullet -}$, 1.251 Å and 133.3° (compared to the experimental values of 1.250 Å and 134°[26]). In the other models, those values of the CO_2 molecule were almost the same as those of free CO_2 molecule, 1.170 Å (compared to the experimental value of 1.162 Å[26]). The total atomic charges of CO_2 in the BN model were larger than those in the other models. The results suggest that the back-donation of electron from Cd atom to CO_2 molecule occurs, forming negatively charged CO_2. In the electron-accepted models, the negative charge of CO_2 was increased through bidentate-type adsorption (BA), while the other type models were comparable with the neutral state models. These results indicate that electron transfer from the

SCHEME 3

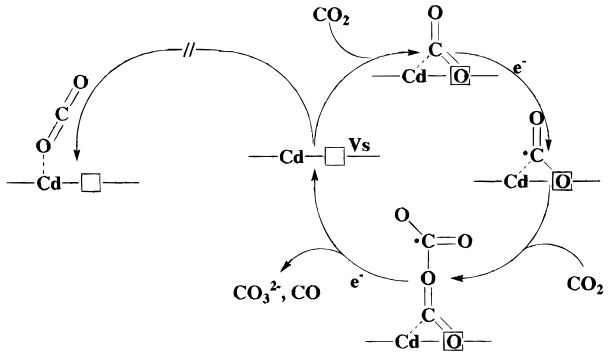

electron-accepted CdS to absorbed CO_2 might proceed with the bidentate-type adsorption on the S-defect surface.

The strong interaction shown in the bidentate-type absorption supports the importance of surface sulfur vacancy in adsorption of CO_2 molecules on the surface of CdS nanocrystallites. The localized charge on CO_2 molecule in the BA model indicates that the next electron transfer to CO_2 may be easy to proceed on the surface with sulfur vacancies.

Mechanism of Photoreduction of CO_2 Molecules. The importance of sulfur vacancies are derived from the following observations and facts: (1) The photocatalytic activity for CO production was increased when 0.2 equivalent amount of excess Cd^{2+} was added into the system, (2) the results from emission and EXAFS measurements supported that the sulfur vacancies on CdS−DMF surface are formed by reaction with the added Cd^{2+} in the systems, (3) MO calculations with the DF method supported the strong interaction between CO_2 molecule and CdS surface with sulfur vacancies through bidentate-type adsorption of CO_2. From these points of view, the Cd atoms in the vicinity of sulfur vacancies should act as adsorptive sites for CO_2 molecule. According to these results, we postulate here a mechanism for the photoreduction of CO_2 to CO on the CdS−DMF nanocrystallites by focusing the importance of sulfur vacancies (Scheme 3).

Upon visible light irradiation of the CdS−DMF system, the photoformed electron on the conduction band migrates to the adsorbed CO_2, forming adsorbed $CO_2^{\bullet-}$ on Cd atoms of CdS−DMF nanocrystallites, where CO_2 interacts with the Cd atom through the C and O atoms. On the surface of CdS−DMF with sulfur vacancies, $CO_2^{\bullet-}$ may accept successive electrons after forming a $Cd^{2+}OCOCO_2$ complex through reaction with another CO_2. This complex may be reduced, leading to CO elimination, as has been reported in electrical CO_2 reduction to CO.[27]

Conclusion

Mechanistic investigation of CdS photocatalytic system for CO_2 reduction was carried out in view of surface structures of the CdS nanocrystallites and CO_2 molecules. The present system is characterized by drastic improvement of photocatalytic activity through the formation of sulfur vacancies. The formation of sulfur vacancies on CdS−DMF nanocrystallites was confirmed by the static and dynamic emission measurements, and in situ Cd K-edge EXAFS analysis. Adsorptive interaction between the surface of the nanocrystallites and CO_2 molecules was confirmed by the increment of emission intensity and the elongation of lifetime of the emission. MO calculations also supports the adsorptive interaction on the CdS surface with sulfur vacancies. The CO formation process via adsorption of CO_2 to Cd atom in the vicinity of sulfur vacancy was newly proposed.

Acknowledgment. We wish to thank Dr. S. Kishimoto at the National Laboratory for High Energy Physics for performing EXAFS measurements. This work was supported in part by Grants-in-Aid for Scientific Research from the Ministry of Education, Science, Sports, and Culture, Japan (Nos. 06403023, 08232253, 07740462), and by a Research Fellowship for Young Scientists from the Japan Society for the Promotion of Science (to H.F.).

References and Notes

(1) Semiconductor Photocatalysis. Part 23. Part 22: Yanagida, S.; Kanemoto, M.; Ishihara, K.; Wada, Y.; Mori, H. *Bull. Chem. Soc. Jpn.*, in press.

(2) Halmann, M. M. *Chemical Fixation of Carbon Dioxide' Methods for Recycling CO_2 into Useful Products*; CRC Press: Boca Raton, FL, 1993, and references therein.

(3) Kanamoto, M.; Ishihara, K.; Wada, Y.; Sakata, T.; Mori, H.; Yanagida, S. *Chem. Lett.* **1992**, 835.

(4) (a) Kanemoto, M.; Shiragami, T.; Pac, C.; Yanagida, S. *Chem. Lett.* **1990**, 931. (b) Inoue, H.; Torimoto, T.; Sakata, T.; Mori, H.; Yoneyama, H. *Chem. Lett.* **1990**, 1483. (c) Kanemoto, M.; Shiragami, T.; Pac, C.; Yanagida, S. *J. Phys. Chem.* **1992**, *96*, 3521. (d) Kanemoto, M.; Hosokawa, H.; Wada, Y.; Murakoshi, K.; Yanagida, S.; Sakata, T.; Mori, H.; Ishikawa, M.; Kobayashi, H. *J. Chem. Soc., Faraday Trans.* **1996**, *92*, 2401.

(5) Inoue, H.; Moriwaki, H.; Maeda, K.; Yoneyama, H. *J. Photochem. Photobiol. A: Chem.* **1995**, *86*, 191.

(6) Inoue, H.; Liu, B.; Sakata, T.; Mori, H.; Yoneyama, H. *Chem. Lett.* **1994**, 653.

(7) (a) Henglein, A.; Gutiérrez, M. *Ber. Bunsen-Ges. Phys. Chem.* **1983**, *87*, 852. (b) Nedeljkovc, J. M.; Nenadovi, M. T.; Micic, D. I.; Nozik, A. *J. Phys. Chem.* **1986**, *90*, 12. (c) Anpo, M.; Kodama, S.; Kubokawa, Y. *J. Phys. Chem.* **1987**, *91*, 4305. (d) Bahnemann, D. W.; Kormann, C.; Hoffmann, M. R. *J. Phys. Chem.* **1987**, *91*, 3789. (e) Spanhel, I.; Haase, M.; Weller, H.; Henglein, A. *J. Am. Chem. Soc.* **1987**, *109*, 5649. (f) Yanagida, S.; Ishimaru, Y.; Miyake, Y.; Shiragami, T.; Pac, C.; Hashimoto, K.; Sakata, T. *J. Phys. Chem.* **1988**, *92*, 3476. (g) Shiragami, T.; Pac, C.; Yanagida, S. *J. Phys. Chem.* **1990**, *94*, 504.

(8) (a) Sakaki, S.; Kitaura, K.; Morokuma, K. *Inorg. Chem.* **1982**, *21*, 760. (b) Sakaki, S.; Dedieu, A. *Inorg. Chem.* **1987**, *26*, 3278. (c) Sakaki, S.; Dedieu, A. *J. Organomet. Chem.* **1986**, *314*, C63. (d) Sakaki, S.; Koga, N.; Morokuma, K. *Inorg. Chem.* **1990**, *29*, 3110.

(9) (a) Beley, M.; Collin, J.; Ruppert, R.; Sauvage, J. *J. Am. Chem. Soc.* **1986**, *108*, 7461. (b) Sakaki, S. *J. Am. Chem. Soc.* **1990**, *112*, 7813. (c) Sakaki, S. *J. Am. Chem. Soc.* **1992**, *114*, 2055. (d) Ogata, T.; Yanagida, S.; Brunschwig, B. S.; Fujita, E. *J. Am. Chem. Soc.* **1995**, *117*, 6708.

(10) Hashimoto, K. *Photochemistry (in Japanese)* **1991**, *15*, 26.

(11) Hosokawa, H.; Fujiwara, H.; Murakoshi, K.; Wada, Y.; Yanagida, S.; Satoh, M. *J. Phys. Chem.* **1996**, *100*, 6649.

(12) Hosokawa, H.; Murakoshi, K.; Wada, Y.; Yanagida, S.; Satoh, M. *Langmuir* **1996**, *12*, 3598.

(13) Teo, B. K. *EXAFS: Basic Principales and Data Analysis*; Springer-Verlag: Berlin, 1986. (b) Koningsberger, D. C.; Prins, R. *X-ray Absorption: Principles, Applications, Techniques of EXAFS, SEXAFS and XANES*; Wiley: New York, 1988. (c) Sakane, H.; Miyanaga, T.; Watanabe, N.; Ikeda, S.; Yokoyama, Y. *Jpn. J. Appl. Phys.* **1988**, *110*, 3763. (d) Mckale, A. G.; Veal, B. W.; Paulicas, A. P.; Chan, S. K.; Knapp, G. *J. Am. Chem. Soc.* **1988**, *110*, 3763. (e) Lytle, F.; Sayers, D. E.; Stern, E. A. *Physica B* **1989**, *158*, 701.

(14) Salahub, D. R.; Fournier, R.; Papai, I.; St-Amant, A.; Ushio, J. *Density Functional Methods in Chemistry*; Springer-Verlag: Berlin, 1991.

(15) (a) Ramsdem, J. J.; Gräetzel, M. *J. Chem. Soc., Faraday Trans.* **1984**, *80*, 919. (b) Brus, L. E. *J. Phys. Chem.* **1986**, *90*, 2555. (c) O'Neil, M.; Marohn, J.; McLendon, G. *J. Phys. Chem.* **1990**, *94*, 4356.

(16) (a) Weller, H.; Koch, U.; Gutiérrez, M.; Henglein, A. *Bunsen-Ges. Phys. Chem.* **1984**, *88* 649. (b) Spanhel, L.; Weller, H.; Fojtik, A.; Henglein, A. *Bunsen-Ges. Phys. Chem.* **1987**, *91*, 88.

(17) (a) Gutiérrez, M.; Henglein, A. Ber. *Bunsen-Ges. Phys. Chem.* **1983**, *87*, 474. (b) Shiragami, T.; Ankyu, H.; Fukami, S.; Pac, C.; Yanagida, S.; Mori, H.; Fujita, H. *J. Chem. Soc., Faraday Trans.* **1992**, *88*, 1055. (c) Shiragami, T.; Fukami, S.; Pac, C.; Yanagida, S. *J. Chem. Soc., Faraday Trans.* **1993**, *89*, 1857. (d) Shiragami, T.; Fukami, S.; Wada, Y.; Yanagida, S. *J. Phys. Chem.* **1993**, *97*, 12882.

(18) (a) Fojtik, A.; Weller, H.; Koch, U.; Henglein, A. *Ber. Bunsen-Ges. Phys. Chem.* **1984**, *88*, 969. (b) Chestony, N.; Harris, T. D.; Hull, R.; Brus, L. E. *J. Phys, Chem.* **1986**, *90*, 3393. (c) Weller, H.; Schmidt, H. M.; Koch, U.; Fojtik, A.; Barl, A.; Henglein, A.; Kunath, W.; Weiss, W.; Dieman, E. *Chem. Phys. Lett.* **1986**, *124*, 969. (d) Hodes, G.; Alubu-Yaraon, A.; Decker, F.; Motisuke, P. *Phys. Rev. B* **1987**, *36*, 4215. (e) Dunstan, D. E.; Hagfeldt, A.; Almgren, M.; Siegbahn, H. O. G.; Mukhatar, E. *J. Phys. Chem.* **1990**, *94*, 6797. (f) Eychmüller, A.; Hasselbarth, A.; Katsikas, L.;

Weller, H. *Ber. Bunsen-Ges., Phys. Chem.* **1991**, *95*, 79. (g) Kamat, P. V.; Patrick, B. *J. Phys. Chem.* **1992**, *96*, 6829.

(19) Assuming three-component decay fitting as follows: $F(t) = a_1 \exp(-t/\tau_1) + a_2 \exp(-t/\tau_2) + a_3 \exp(-t/\tau_3)$. Average lifetime of the emission was calculated using the parameters given by the three-component fitting. The average lifetime is defined as used in previous reports (Jamaes, D. R.; Liu, Y.-S.; Mayo, P. De.; Ware, W. R. *Chem. Phys. Lett.* **1985**, 120, 460). τ_{ave}: $[\tau] = \sum a_i\tau_i^2/\sum a_i\tau_i$.

(20) Ozutsymi, K.; Takamuku, T.; Ishiguro, S.; Ohtaki, H. *Bull. Chem. Soc. Jpn.* **1989**, *62*, 1875.

(21) The extracted reference parameters were as follows: Cd−O shell: ΔE_0, 7.753 eV; $\eta_j(k)$, 1.238 Å^{-2}; $S_j(k)$, 0.907; C_j, 7.742 rad; Cd−S shell: ΔE_0, 5.927 eV; $\eta_j(k)$, 1.031 Å^{-2}; $S_j(k)$, 0.894; C_j, 1.637 rad. The function used to fit the data is the following:[11,13] $\chi(k) = \sum\{N_jS_j(k)F_j(k)/kr_j^2\}\exp(-2\sigma_j^2k^2)\exp(-2r_j\eta_j(k)/k)\sin(2kr_j + \phi(k) - k^3C_j)$, $k = 2\pi\{2m_e(E - E_0)^{1/2}\}/h$.

(22) Marcus, M. A.; Brus, L. E.; Murray, C.; Bewendi, M. G.; Prasad, A.; Alivisatos, A. P. *Nanostruct. Mater.* **1992**, *1*, 323.

(23) Fujiwara, H.; Kanemoto, M.; Ankyu, H.; Murakoshi, K.; Wada, Y.; Yanagida, S. *J. Chem. Soc., Parkin Trans. 2* **1997**, 317.

(24) The ideal surface and the S-defect surface was abbreviated the first letter of the acronyms as I and D, respectively. O-end-on models, C-adsorbed models, and bidentate-type model of adsorbed CO_2 was abbreviated with the second letter of the acronyms as O, C, and B, respectively. The neutral states and the electron-accepted states were abbreviated with the third letter of the acronyms as N and A, respectively.

(25) Risk, J.; Solymosi, F. *J. Phys. Chem.* **1994**, *98*, 7147.

(26) Herzberg, G. *Molecular Spectra and Molecular Structure, III. Electronic Spectra and Electronic Structure of Polyatomic Molecules*; Van Nostrand: London, 1967.

(27) (a) Gressin, J. C.; Michelet, D.; Nadjo, L.; Savéant, J. *Nouv. J. Chem.* **1977**, *3*, 545. (b) Amatore, C.; Savéant, J. *J. Am. Chem. Soc.* **1981**, *103*, 5021.